Materials Science in Semiconductor Processing 174 (2024) 108161

Contents lists available at ScienceDirect

Materials Science in Semiconductor Processing

journal homepage: www.elsevier.com/locate/mssp

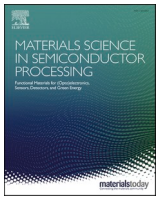

Comparison of one and two-stage growth approaches for close space sublimation deposition of Sb_2Se_3 thin film solar cells

Daniya A. Sindi [a,b,*], Thomas P. Shalvey [a], Jonathan D. Major [a]

[a] Department of Physics and Stephenson Institute for Renewable Energy, University of Liverpool, Liverpool, L69 7ZF, UK
[b] Department of Physics, College of Science, Umm Al-Qura University, Makkah, Saudi Arabia

A B S T R A C T

In this work, we investigate the impact of grain structure and ribbon orientation on Sb_2Se_3 solar cells deposited by close space sublimation (CSS). Films of Sb_2Se_3 were produced using either a single-stage low-temperature "seed-layer" deposition, a high-temperature "growth-layer" deposition, or a combined two-stage deposition process combining both "seed" and "growth" layers. This study demonstrates the essential nature of the "seed" layer to achieve the required substrate coverage and ensure functioning Sb_2Se_3 solar cells by this technique. A photovoltaic efficiency of 5.07 % was obtained by fabricating solar cells with a two-stage Sb_2Se_3 growth process using the structure (FTO/TiO_2/Sb_2Se_3/P3HT/Au) in superstrate configuration. Comparisons were made between device performance and ribbon orientation assessed by XRD measurements via a ribbon carrier transport (RCT) analysis method, as well as with surface coverage and grain size. The addition of a second growth stage was found to result in a more vertical ribbon orientation compared to a single low temperature deposition, however predominantly controls the overall surface coverage. We observe no obvious links between the orientation of ribbons and the cell performance. Instead we propose that the performance, and in particular the device V_{OC}, is more strongly determined by the overall grain structure rather than simply by the ribbon orientation.

1. Introduction

Thin film solar cells including CdTe, Cu(In,Ga)Se_2 (CIGS), and MAPI perovskite, have achieved relatively high levels of efficiency and industrial implementation. However each technology has it is own concerns, the scarcity of Te, In, and Ga and the toxicity associated with Cd and Pb present limitations [1]. $Cu_2ZnSn(Se,S)_4$ has long been considered a promising material due to its low cost and non-toxic constituent elements [2]. Unfortunately, the presence of carrier trapping defects and the complex phase composition have limited efficiency progression [3,4]. Simple binary chalcogenides which can be more reliably produced appeal as alternative absorbers, particularly if they have lower toxicity, and good abundance [1]. A prime example of such a material is antimony selenide (Sb_2Se_3) which has made significant strides. It exhibits desirable characteristics such as a near optimal band gap with a particularly high absorption coefficient [5–8]. The current champion device for Sb_2Se_3 thin-film solar cells stands at 10.57 % [9] but there is significant scope for further development given spectroscopy limited maximum efficiency (SLME) and radiative limit calculations suggest an upper limit of >30 % [10,11].

The structure of Sb_2Se_3 consists of a one-dimensional nanoribbon lattice, formed via $(Sb_4Se_6)_n$ units that are interconnected through van der Waals forces in the [010] and [100] directions. In contrast, the units are held together through strong covalent bonds in the [001] direction [12,13]. This anisotropic bonding has been proposed to result in direction-dependent carrier transport properties [13]. Theoretical calculations indicate that (110) and (120) surfaces possess components which have lower formation energies and are terminated with non-dangling bonds [14]. Consequently, there is a propensity for Sb_2Se_3 grains to grow with their c-axis parallel to the junction [15], although absorber layers comprising of vertically aligned Sb_2Se_3 ribbons perpendicular to the junction should, theoretically, exhibit favourable carrier extraction and thus device performance. This has previously been observed to an extent via a negative correlation between device efficiency and (120) orientation in films which is attributed to a higher series resistance [14]. In this work we have used the space group #62 Pbnm setting for the Miller indexing of planes in Sb_2Se_3 for which a = 11.648, b = 11.794 and c = 3.986 Å and the covalently bonded ribbons lie parallel to the c-vector, [001] [16].

Growth of Sb_2Se_3 thin films by high temperature physical vapor deposition (PVD) techniques such as close space sublimation (CSS) can be highly challenging. As well as typical requirements of a compact, dense, pinhole-free [17] film structure, there is also the perceived need to achieve a preferential ribbon orientation. A large focus of the research field to date has been to optimize the orientation of ribbons to maximize carrier transport and reduce grain boundary recombination [18,19].

* Corresponding author. Department of Physics and Stephenson Institute for Renewable Energy, University of Liverpool, Liverpool, L69 7ZF, UK.
E-mail address: d.a.m.sindi@liverpool.ac.uk (D.A. Sindi).

https://doi.org/10.1016/j.mssp.2024.108161
Received 26 October 2023; Received in revised form 12 January 2024; Accepted 21 January 2024
Available online 8 February 2024

This has been shown to have links to deposition conditions [20,21] hence is often a key consideration when determining optimal growth parameters. Despite the potential of less problematic grain boundary behaviour [22], it may still be beneficial to achieve large grain sizes. Whilst grain boundaries in Sb_2Se_3 may be less harmful recombination centres they may still act to channel carriers [22], meaning grains which extend the full thickness of the film are required.

The evidence for strongly anisotropic electronic properties of Sb_2Se_3 is conclusive, however it remains unclear the extent to which the grain orientation of films impacts the overall performance of solar cells. The anisotropic carrier mobility in particular is assumed to result in a significantly higher resistivity of films with a strong (hk0) orientation compared to those without. However, although the *ratio* of resistivity between the different crystallographic directions might be sizeable, the total *absolute* resistivity this adds to a device stack, and therefore it's importance for Sb_2Se_3 solar cells (especially at this stage in their development) might not. Given the highest efficiency devices tend to be solution processed at relatively low temperature, and therefore comprise of a relatively large fraction of grains parallel to the substrate, the additional series resistance this imparts would be expected to most severely reduce short circuit current density. However, this does not appear to be the case, with 33.52 mA cm^{-2} output from a device with large (hk0) diffraction peaks compared to a detailed balance limit of ~40 mA cm^{-2}, despite parasitic absorption from the glass substrate, transparent electrode and a relatively thick CdS layer [9]. Indeed, there are numerous instances of devices with strong hk0 peaks which have current densities approaching the detailed balance limit, with the remaining deficit largely due to optical losses in other parts of the device stack [23]. This suggests Sb_2Se_3 solar cells can achieve very high current densities in spite of many hk0 orientated grains, which raises the question of whether the emphasis placed on grain orientation engineering in literature is well founded.

The primary limits to higher efficiency Sb_2Se_3 devices are unambiguously open circuit voltage (V_{oc}) and fill factor (FF). Whilst carrier mobility (and by extension any anisotropy due to crystal structure) can influence V_{oc}, this is not the argument put forward in most reports, and there is no evidence of a strong dependence in literature. Likewise, whilst the fill factor will be affected by series resistance, this does not seem to be the dominant restriction for Sb_2Se_3 solar cells. For example, we calculate the literature record CdTe device [24] ($\eta = 20.8$ %, FF = 79.8 %) to have a series resistance of ~2.02 Ω cm^{-2} compared to 2.23 Ω cm^{-2} for the record Sb_2Se_3 device [9] ($\eta = 10.57$ %, FF = 67.64 %) which has a strong hk0 orientation component. Clearly then, the series resistance does not appear to be the limiting factor to higher efficiencies at present.

Our group has previously established a two-stage growth process including a "seed" layer followed by a main "growth" layer to achieve good film coverage and grain structure [13]. However, the relative benefits/limitations of seed and main layer growth have not been fully established. This work seeks to compare device series which separate the two stages and establish the level to which they control grain structure, ribbon orientation and device performance. We report a comparison of device performance with grain size, substrate coverage and the ribbon orientation of all samples determined using a simplified ribbon carrier transport (RCT) metric proposed by Pattini et al. [20]. Whilst the use of lower temperature deposition steps remains essential for coverage we find no discernible correlation between Sb_2Se_3 film orientation, growth conditions and photovoltaic device performance. We show that while good performance can be achieved using a single low temperature deposition step there is a minor performance benefit by the addition of a second higher temperature growth step.

2. Experimental section

2.1. Synthesis of Sb_2Se_3 thin-film solar cells

A device structure of FTO/TiO_2/Sb2Se_3/P3HT/Au was used with TEC15 SnO_2:F (FTO) coated soda-lime glass acting as both the substrate and transparent electrode. TiO_2 precursor solutions were prepared inside a nitrogen-filled glovebox with two concentrations of 0.15 M and 0.3 M, by the addition of 45 μl or 90 μl of titanium isopropoxide (TTIP) to 1 ml ethanol. 10 μl or 20 μl of an acetic acid catalyst was added for 0.15 M and 0.3 M concentrations respectively before stirring at 400 rpm for 1 h. Finally, the TiO_2 solutions were filtered into new bottles prior to deposition to remove particulates. TiO_2 films with a thickness of ~50 nm were deposited on FTO glass substrate via spin coating. 200 μl of a the 0.15 M TTIP solution was deposited at 1000 rpm for 10 s followed by 3000 rpm for 30 s. After evaporating the residual solvent by placing the samples on a hotplate at 110 °C for 10min, the process was repeated for the 0.3 M TTIP solution. The TiO_2 films were then annealed at 500 °C for 30 min in air to recrystallize the films into an anatase phase [25].

The Sb_2Se_3 absorber layer was then deposited onto the TiO_2 layers via either a one or two-stage close space sublimation process to separate the effect of each step on the cell performance. The lower temperature step we refer to as the "seed" layer with the higher temperature step referred to as the "growth" layer. Here we compare three separate samples sets:

Set A - single "growth" layer: Sb_2Se_3 was deposited by pre-heating the source and substrate at 350 °C for 20 min under vacuum, with no deposition occurring at this temperature. The "growth" layer was the deposited with a 530 °C source temperature and 490 °C substrate temperature, with deposition times ranging between 1 and 10 min, under a backfilled pressure of 10 Torr N_2.

Set B - single "seed'' layer: Sb_2Se_3 layers were deposited with the source temperatures varied between 440 °C and 400 °C, whilst the substrate temperature was between 390 °C and 350 °C. The growth times were modified to achieve comparable thickness of ~ 600 nm ± 50 nm in each case, and depositions were carried out under vacuum.

Set C - Fixed "seed' with varied "growth" layers substrate temperatures: Finally, a set of samples were produced where the seed layer was deposited with a source temperature of 440 °C and substrate temperature of 350 °C under vacuum for 17 min. Then a second "growth" layer step was then deposited with a source temperature of 530 °C, substrate temperature of either 490 °C or 420 °C, and with deposition time between 1 and 10 min under 10 Torr N_2. This allowed a wide range of growth conditions to be compared and the impact on device performance and ribbon orientation to be assessed.

All samples were processed into solar cells using identical back contact processing of a P3HT organic hole transport layer, followed by a metal Au contact. A 10 mg/ml P3HT solution in chlorobenzene was prepared in a nitrogen filled glovebox. 100 μl of this solution was spin coated onto the Sb_2Se_3 back surface in air at 1000 rpm for 10s followed by 3000 rpm for 30s. Finally, Au was deposited by thermal evaporation as the back contact at a thickness of 50 nm at room temperature.

2.2. Characterization

Surface morphologies and elemental analysis of the films were observed by scanning-electron microscopy (SEM) and energy dispersive spectroscopy (EDS) using a JEOL JSM 7001F. The microstructure of films was investigated by calculating the average grain size and the coverage which were determined by manually tracing the grain boundary edges, which can be analysed using ImageJ to calculate the area of each individual grain [26].

X-ray diffraction (XRD) was carried out with monochromated Cu Kα radiation ($\lambda = 1.5406$ Å) to characterize the crystal structure of the samples using a Rigaku SmartLab system in parallel beam geometry. Current-voltage (JV) measurements were taken under AM1.5

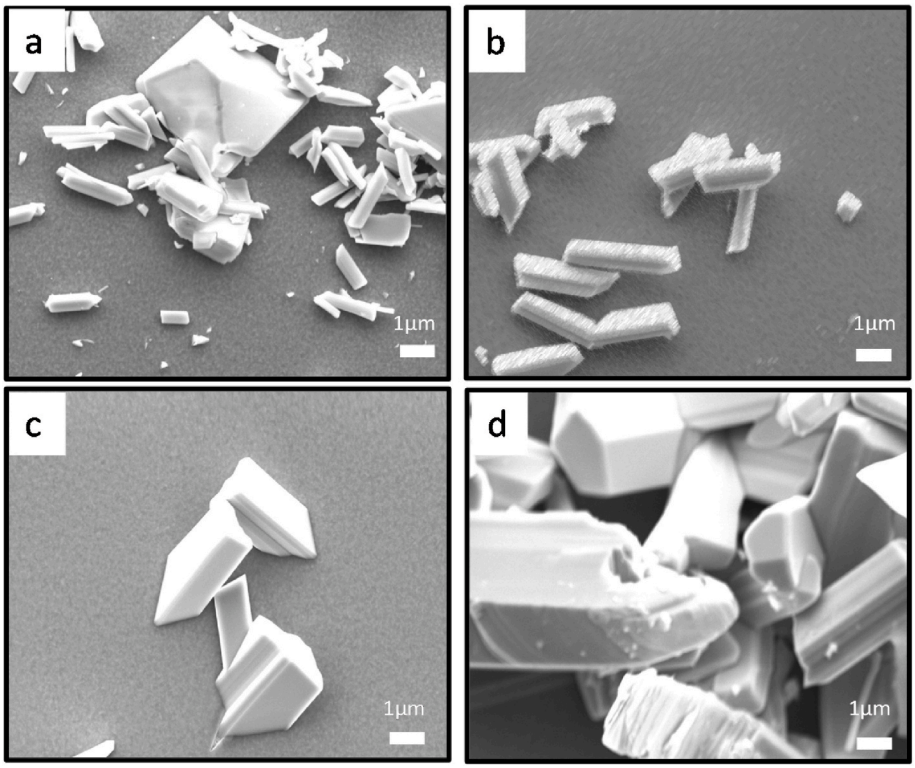

Fig. 1. SEM image of "growth" layer films deposited at T_{source} = 530 °C and $T_{substrate}$ = 490 °C for a)1 min b) 2 min c) 4 min and d) 10 min, all under 10 Torr nitrogen.

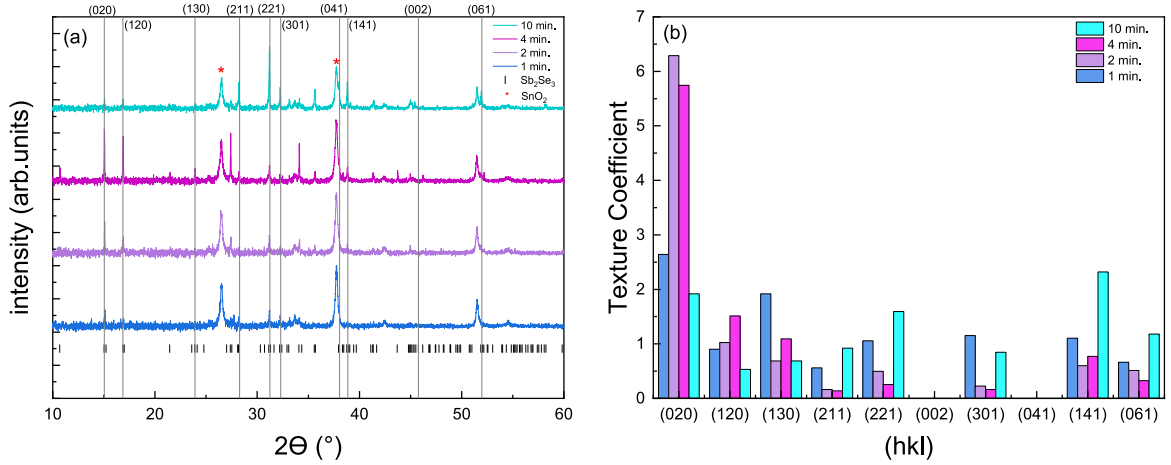

Fig. 2. a) XRD patterns recorded for TiO_2/Sb_2Se_3 structures using "growth" layer conditions with different deposition time and b) texture coefficient determined from XRD patterns for each sample. The main index surfaces for Sb_2Se_3 used for RCT analysis, any peaks not labelled are also from Sb_2Se_3.

illumination using a TS Space Systems solar simulator (class AAA). A Keithley 2400 source-measure unit recorded the output current for measurement for bias range of -1V to +1V for each scan at room temperature. External quantum efficiency (EQE) measurements were taken using a Bentham PVE300 device calibrated with a silicon photodiode. A 300–1100 nm range was used with no white light biasing applied.

3. Result and discussion

3.1. Deposition of Sb_2Se_3 on hot substrate with various "growth" layers conditions

The overall focus of this study is to identify key CSS deposition conditions for Sb_2Se_3 thin-film absorbers and solar cells. The intention is to determine preferable processing conditions for grain growth and orientation, and to understand their relation with the device's performance. As a first stage of this a series of cells were produced which had a single high temperature deposition step. Such a high temperature "growth" layer step is often used during CSS deposition of Sb_2Se_3 to encourage a large grain structure by recrystalising material pre-deposited during a lower temperature growth stage [13]. Here we consider this layer in isolation however in order to gain an understanding of the quality of the layers produced, but in the expectation film structure was likely to be unsuitable.

Sb_2Se_3 layers were deposited on TEC15/TiO_2 underlayers using deposition conditions of T_{Source} = 530 °C with T_{Sub} = 490 °C for 1, 2, 4

Table 1
TC and RCT values determined from XRD analysis for Sb_2Se_3 (hkl) orientations studied for samples prepared with "Growth" conditions for different deposition time.

Deposition time		*020	*120	*130	*211	*221	*002	*301	*041	*141	*061	$\Sigma TC_{(hk0)}$	$\Sigma TC_{(hkl)\ l\neq 0}$	ΣRCT (%)
1 min	TC	2.6	0.9	1.9	0.6	1.1	0.0	1.2	0.0	1.1	0.7	5.5	4.5	
	RCT	0.0	0.0	0.0	0.4	0.8	0.0	0.8	0.0	0.6	0.3			2.9
2 min	TC	6.3	1.0	0.7	0.2	0.5	0.0	0.2	0.0	0.6	0.5	8.0	2.0	
	RCT	0.0	0.0	0.0	0.1	0.4	0.0	0.2	0.0	0.3	0.2			1.2
4 min	TC	5.7	1.5	1.1	0.1	0.3	0.0	0.2	0.0	0.8	0.3	8.3	1.7	
	RCT	0.0	0.0	0.0	0.1	0.2	0.0	0.1	0.0	0.4	0.1			1.0
10 min	TC	1.9	0.5	0.7	0.9	1.6	0.0	0.8	0.0	2.3	1.2	3.1	6.9	
	RCT	0.0	0.0	0.0	0.7	1.1	0.0	0.6	0.0	1.3	0.5			4.3

Table 2
Sb_2Se_3 crystallographic orientations, their associated ribbon angles relative to the surface normal, and the effective vertical component (EVC) of each ribbon direction.

Crystallographic Orientation	Ribbon angle relative to surface normal (∘)	Effective Vertical Component (EVC)
(002)	0	1
(211)	37.3	0.79
(221)	43.8	0.72
(301)	45.7	0.70
(041)	53.4	0.60
(141)	54.2	0.58
(061)	63.6	0.44
(hk0)	90	0

and 10 min under 10 Torr of nitrogen. These films were observed to be semi-transparent to the naked eye implying poor substrate coverage. Fig. 1 shows a top down SEM image of the Sb_2Se_3 films deposited for the different deposition times.

It is immediately clear that there is very poor coverage of the substrate using this one stage deposition process. In Fig. 1a, films deposited for 1-min duration show a sparsely populated substrate, covered with elongated rod-like grains, which are characteristic of the Sb_2Se_3 due to its one-dimensional crystal structure. Increasing the deposition time leads to fewer grains, presumably as the material coalesces together, resulting in a slightly larger typical grain size as show in Fig. 1b and c, but the substrate coverage remains poor. Fig. 1d shows the film morphology after increasing the deposition time to 10 min. The substrate coverage was significantly improved, and the film had a much larger grain size, but it is not compact and there are still distinct voids visible, therefore the film structure remains unsuitable for device fabrication.

The same samples were then analysed via XRD to determine the impact of the growth conditions on the $[Sb_4Se_6]_n$ nanoribbon orientation relative to the substrate. Fig. 2 shows XRD patterns of Sb_2Se_3 absorbers with reference patterns for Sb_2Se_3 and underlying SnO_2. The

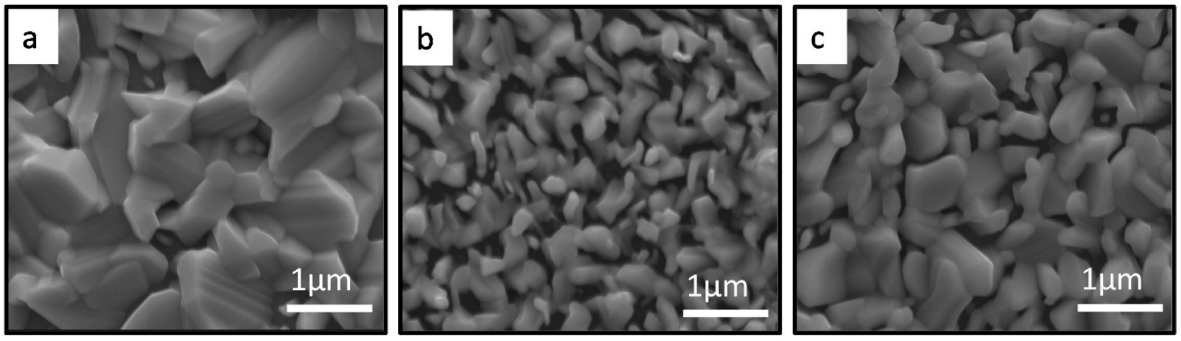

Fig. 3. SEM of Sb_2Se_3 films deposited at a) T_{Source} = 400 °C with T_{Sub} = 350 °C, b) T_{Source} = 440 °C with T_{Sub} = 350 °C and C) T_{Source} = 440 °C with T_{Sub} = 390 °C.

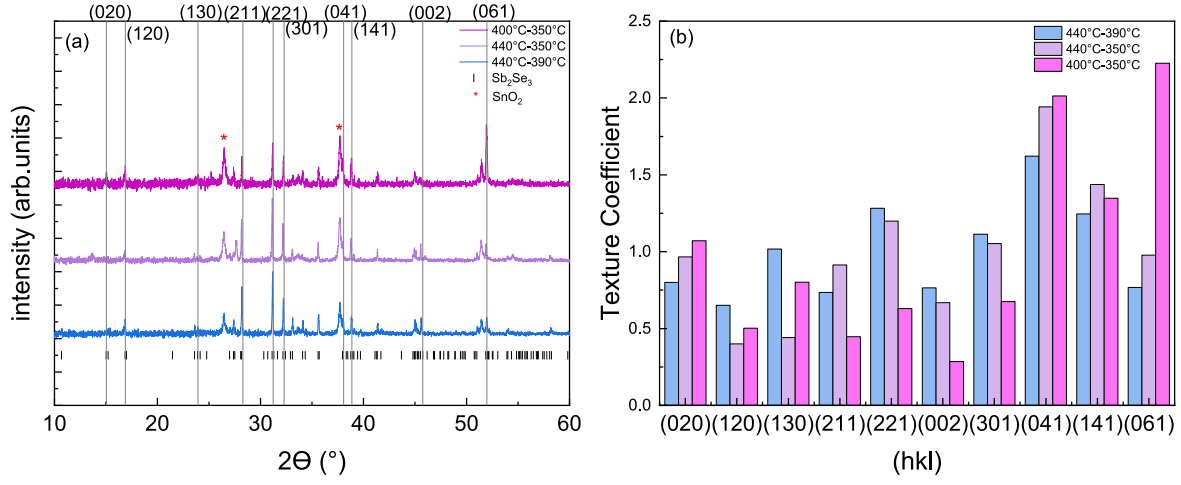

Fig. 4. a) XRD patterns recorded for TiO_2/Sb_2Se_3 with various "seed" deposition conditions and b) texture coefficient analysis determined from XRD patterns.

Table 3
TC and RCT values for Sb_2Se_3 (hkl) orientations studied on "Seed"- layer samples grown at different temperature combinations.

Temperature		020	120	130	211	221	002	301	041	141	061	$\Sigma TC_{(hk0)}$	$\Sigma TC_{(hkl)\ l\neq0}$	ΣRCT (%)
400°C–350 °C	TC	1.1	0.5	0.8	0.4	0.6	0.3	0.7	2.0	1.3	2.2	2.4	7.6	
	RCT	0.0	0.0	0.0	0.4	0.5	0.3	0.5	1.2	0.8	1.0			4.5
440°C–350 °C	TC	1.0	0.4	0.4	0.9	1.2	0.7	1.1	1.9	1.4	1.0	1.8	8.2	
	RCT	0.0	0.0	0.0	0.7	0.9	0.7	0.7	1.2	0.8	0.4			5.4
440°C–390 °C	TC	0.8	0.7	1.0	0.7	1.3	0.8	1.1	1.6	1.2	0.8	2.5	7.5	
	RCT	0.0	0.0	0.0	0.6	0.9	0.8	0.8	1.0	0.7	0.3			5.1

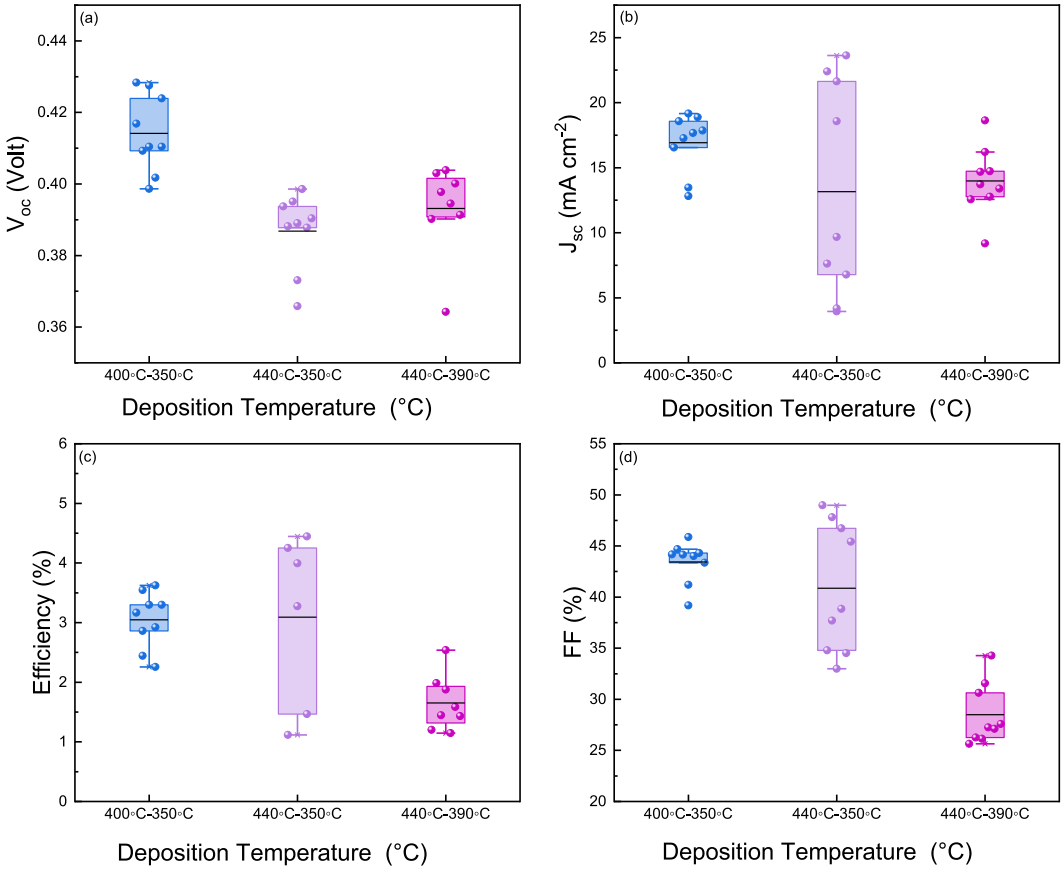

Fig. 5. Cell performance parameters for Sb_2Se_3 "seed" layer devices at various source-substrate temperature combinations a) V_{oc}, b) J_{sc}, c) efficiency and d) FF.

pattern analysis was carried out with respect to orthorhombic structure with *Pbnm* space group symmetry. Analysis of Sb_2Se_3 patterns is complicated by the sheer number of peaks, however it is crucial to assess the impact of anisotropic carrier transport. It has been presumed that orientation with ribbons at normal, or as close to normal as possible, with respect to the junction is preferable for carrier transport. The presence of (hk0) reflections in diffraction patterns is therefore undesirable since they correspond to grains where nanoribbons are oriented parallel to the junction, with (hkl)l≠0 being targeted instead. However, recent theoretical analysis has contradicted this somewhat suggesting Sb_2Se_3 does in fact have quasi-2D carrier transport [10], and it is notable that the current champion device has a significant content of (hk0) texture [9]. A key target of this study was to track the ribbon orientations and relate it to device performance to see if any correlation could be determined.

Firstly, in order to quantify the degree of orientation preference of crystalline planes, the texture coefficient (TC) was calculated according to the Harris' formula [27]:

$$TC(hkl) = \frac{I(hkl)}{I_0(hkl)} \Big/ \frac{1}{N}\sum_{i=1}^{N}\frac{I(h_ik_il_i)}{I_0(h_ik_il_i)}$$

Where (hkl) are the Miller indices, I(hkl)/I_0(hkl) is the ratio of diffraction intensity between a measured thin film and a randomly oriented Sb_2Se_3 powder for a specific peak, and N the number of diffraction peaks considered in the analysis (here N = 10). The presumed undesirably orientated crystal planes whereby the nanoribbons lie flat along the substrate can be identified as (hk0), which are (020), (120) and (130), while the (hkl)l≠0 is represent the other orientations along c-axis direction which are (211), (221), (002), (301), (041), (141) and (061). Fig. 2b shows the determined TC values for each of the four growth times. While there are noticeable changes between the samples, it remains difficult to process the overall impact on the "preferable" ribbon orientations. To further simplify the analysis we have adopted the process established by Pattini et al. [20] where by weighting each TC with an "Effective Vertical Component" (EVC), we can define a "Ribbon

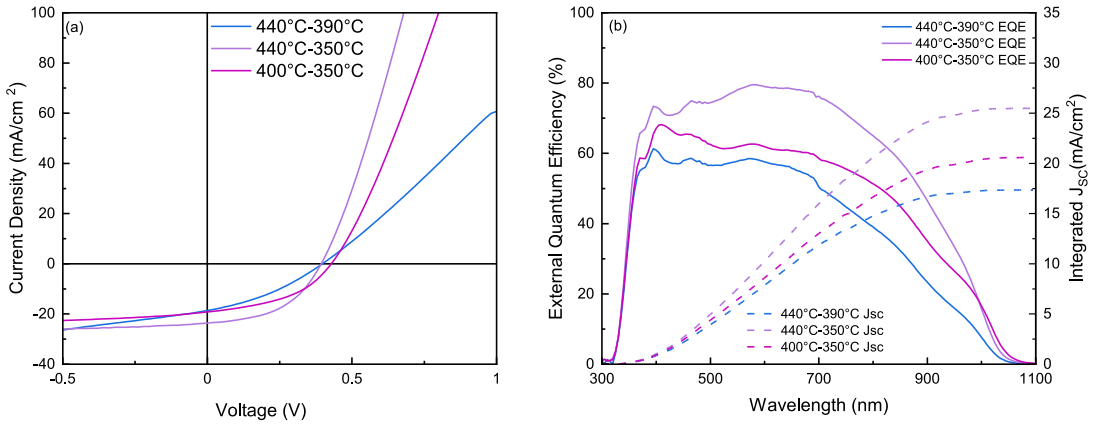

Fig. 6. a) J-V and b) EQE curves for highest efficiency contacts for Sb_2Se_3 devices deposited using a single "seed" layer growth step.

Table 4
PV parameters performance for champion cells.

Samples	V_{OC} [V]	J_{SC} [mA cm^{-2}]	FF [%]	η [%]	R_S [Ω]	R_{SH} [Ω]
440 °C–390 °C	0.39	18.63	34.28	2.54	12.26	10.28
440 °C–350 °C	0.39	23.62	47.81	4.45	4.87	309.89
400 °C–350 °C	0.43	19.17	44.15	3.62	9.59	186.45

Table 5
Film thickness as a function of deposition time and substrate temperature.

Time (min.)	Film Thickness (nm)	
	420 °C	490 °C
1	751	731
2	800	602
4	848	740
10	3100	925

Carrier Transport "(RCT) metric. Where;

$$RCT = TC \times EVC$$

The EVC is calculated by taking the cosine for each orientation angle, the angle formed between the surface normal and the ribbon, e.g. 0° represents vertical and 90° horizontal. The list of the crystallographic orientations, angles and EVC value for the chosen ribbon presented in Table 2. These values are used to calculate ΣRCT, where a larger value reflect a higher angle of orientation relative to the substrate and hence higher values are considered favourable. RCT values are calculated for each sample in Table 1. Comparing the four samples we see that the change in growth time has not had a systematic influence on the overall orientation. All samples compare have a significant (hk0) peaks and samples with the highest TC for these values translate into lower RCT values. RCT is a minimum of 1 at 4 min and 4.3 for the longest deposition time. There is also no presence of the 'ideal' ribbon orientation signified by the (002) texture there but are peaks for the favourable (211) and (221) textures. We note that for some films, in particular those shown in Fig. 1b and c, suggests the peak height from XRD measurements is likely to have large uncertainties associated with them due to limited sampling statistics, resulting from the large grain size combined with sparse

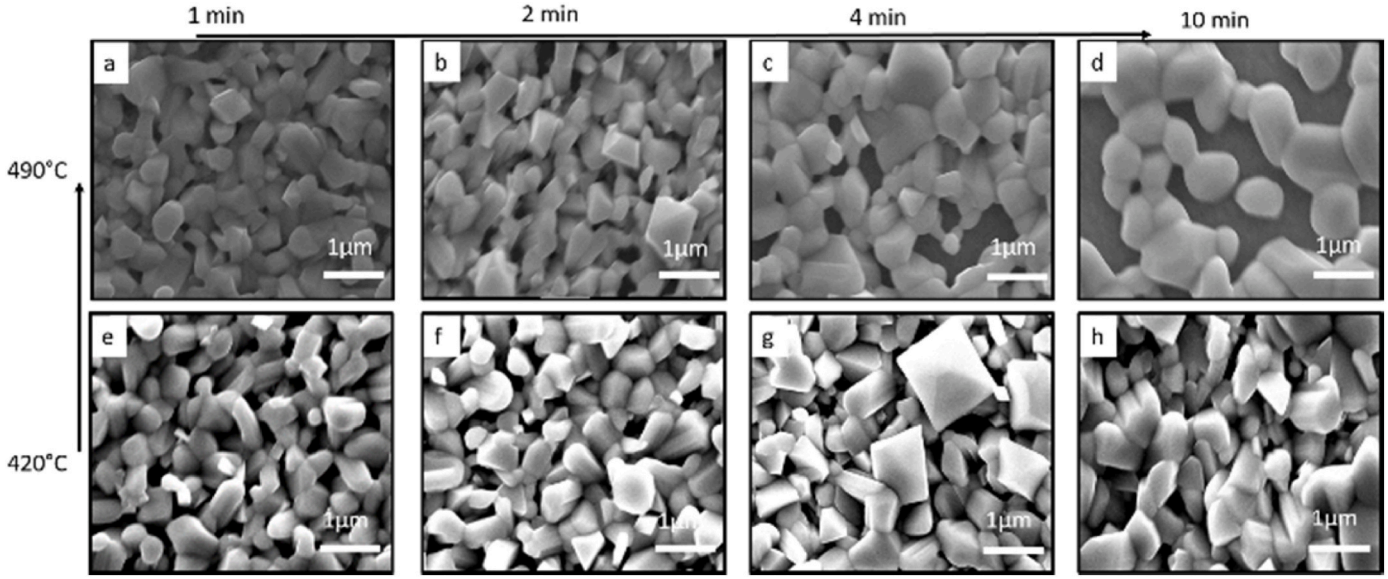

Fig. 7. SEM of films deposited with a growth layer at $T_{substrate}$ 490 °C for a)1min, b) 2min, c) 4min, d)10 min and $T_{substrate}$ = 420 °C for e)1min, f) 2min, g) 4min, h) 10 min.

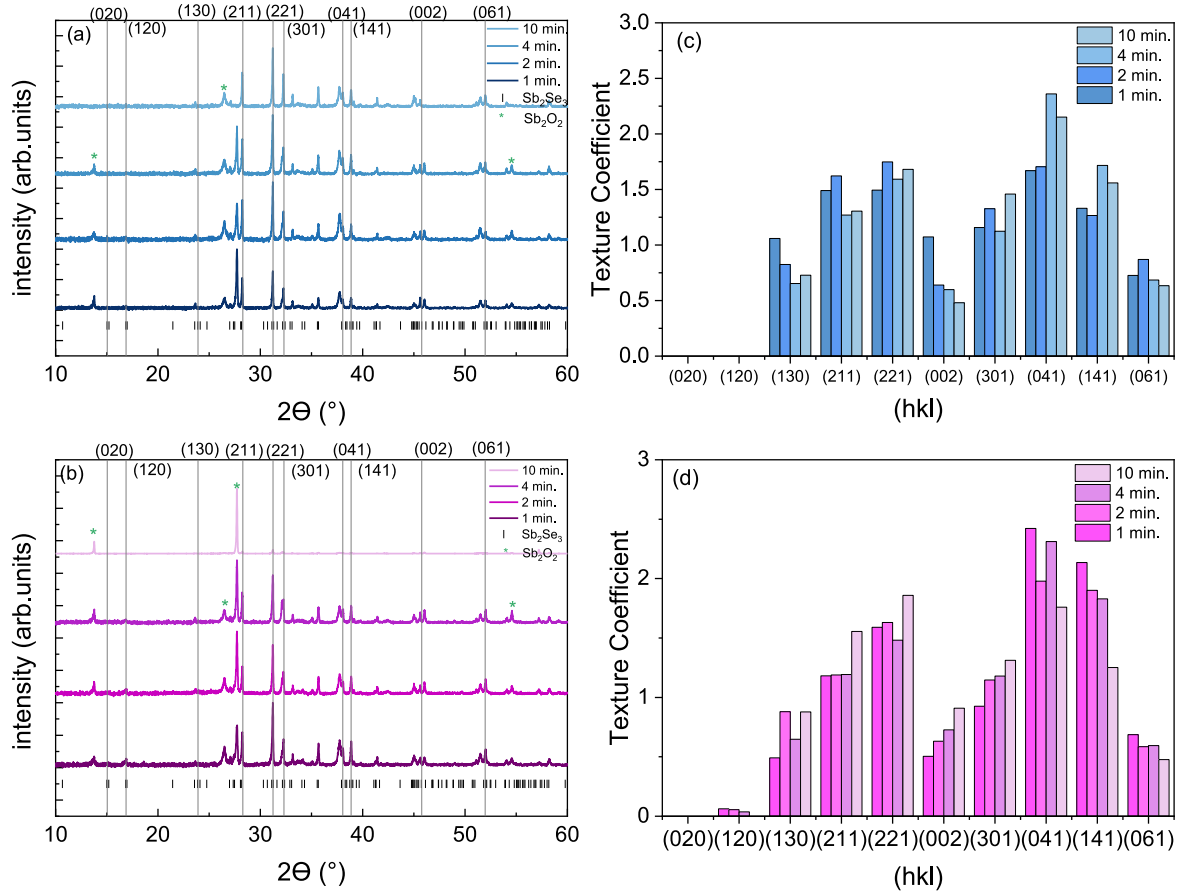

Fig. 8. XRD patterns (a,b) and texture analysis (c,d) of films with a seed layer deposited at T_{source} 440 °C - $T_{substrate}$ 350°C- under vacuum, followed by a growth layer deposited with T_{source} = 530 °C under 10 Torr N_2, and a substrate temperature of either $T_{substrate}$ 490 °C (top) or $T_{substrate}$ 420 °C (bottom).

Table 6
Summary of ΣRCT value for two-stage grown films.

Time (min.)	ΣRCT (%)	
	420 °C	490 °C
1 min.	6.3	6.2
2 min.	6.1	6.2
4 min.	6.3	6.2
10 min.	6.4	6.2

substrate coverage. Nonetheless, given the good agreement between SEM images showing nano-rods lying flat on the substrate, and the (hk0) reflections in the corresponding diffraction patterns, we can conclude that there are sufficient sampling statistics for the purpose of this study. Therefore, the film structure is clearly unsuitable for high performance devices, which highlights that the need for a seed layer step during CSS growth.

3.2. Sb_2Se_3 "seed" layer films

Here devices were produced using a single low temperature "seed" deposition step with three source-substrate temperature combinations compared: i) T_{Source} = 440 °C with T_{Sub} = 390 °C, ii) T_{Source} = 440 °C with T_{Sub} = 350 °C and iii) T_{Source} = 400 °C with T_{Sub} = 350 °C. For each set of conditions, the growth was carried out under vacuum to achieve a workable growth rate and the growth time was modified to produce equivalent thickness of ~600 nm. This sample set was produced in attempt not only to gauge the ability of a single step lower temperature deposition to produce good quality films, but also to compare the respective impact of source and substrate temperature.

Fig. 3 shows top-down SEM images of the three separate Sb_2Se_3 deposition temperature conditions for films on top of FTO/TiO_2. In Fig. 3a films deposited at T_{Source} = 400 °C with T_{Sub} = 350 °C show a defined and reasonably large grain structure. Maintaining the same substrate temperature but increasing the source temperature to 440 °C leads to a reduction in grain size and even more open grain structure with some clear void areas (Fig. 3b). The reduced grain size follows broadly with expectations from the structure zone model and basic thin film nucleation theory [28]. We would anticipate a smaller critical nucleus size due to the faster arrival rate and high adatom mobility for an increased source temperature, producing a film with smaller typical grains [29,30]. Maintaining this high source temperature, but increasing the substrate temperature to 390 °C, Fig. 3c, shows that these films again conform to expectations. The increased substrate temperature increases the adatom surface mobility, thereby increasing the critical radius as well as grain size. Whilst this is broadly in line with expectations from the structure zone model, there is also evidence from literature that the anisotropic growth rate of the crystallographic surfaces has a decisive role in grain size and morphology [31]. Because of the pseudo-1D crystal lattice of Sb_2Se_3 it may be that the material does not conform to the same growth mode patterns as 3D materials in all temperature regimes. Clearly further work is required to develop a complete understanding of the nucleation and growth mechanisms for these low dimensional materials.

Samples in set B were then analysed via XRD in order to determine the influence of the "Seed" layer deposition conditions on the ribbon orientation relative to the substrate. Fig. 4a shows XRD patterns of Sb_2Se_3 absorbers with reference patterns for Sb_2Se_3 and SnO_2. We again conducted analysis of the TC and RCT parameters shown in Fig. 4b and

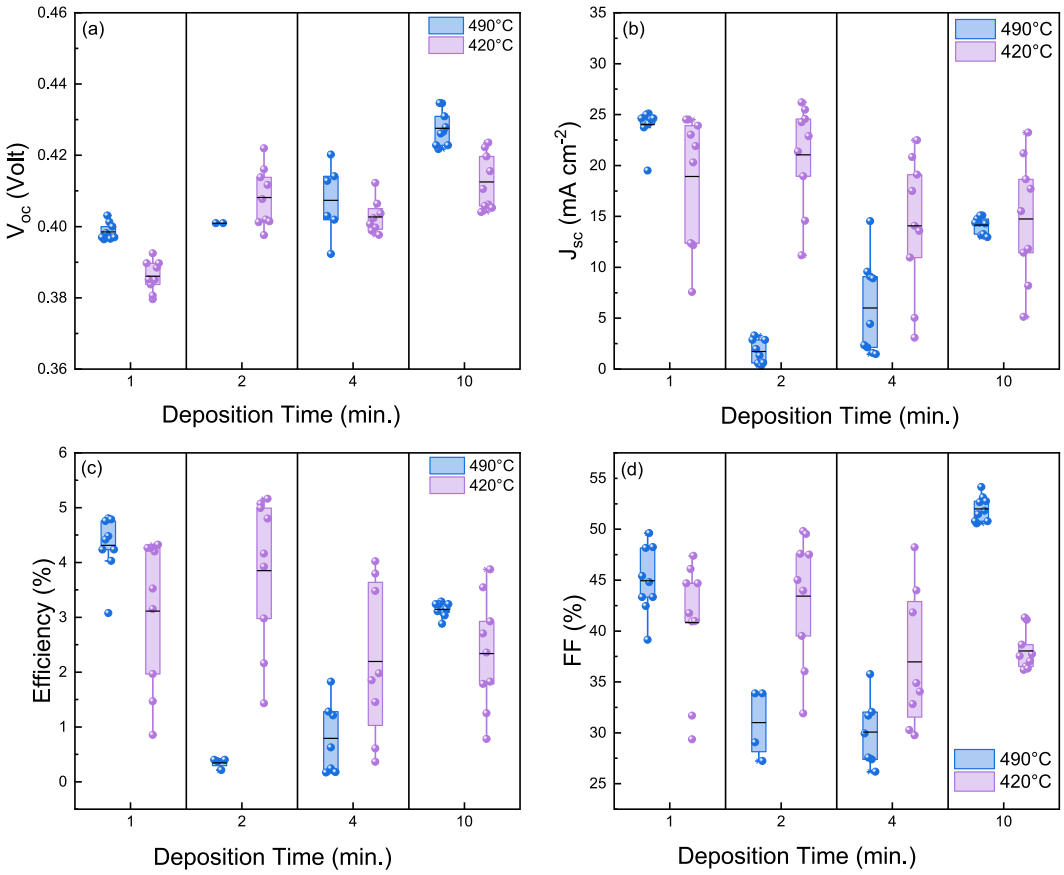

Fig. 9. a) V_{oc}, b) J_{sc}, c) Efficiency and d) FF for cells deposited with a fixed seed layer but varied substrate temperatures and deposition periods.

Table 7
PV parameters performance for champion cells.

Samples	V_{OC} [V]	J_{SC} [mA cm−2]	FF [%]	η [%]	R_S [Ω]	R_{SH} [Ω]
490 °C	0.40	24.14	49.62	4.81	4.85	1050.30
420 °C	0.40	25.47	49.53	5.07	4.89	1249.16

Table 3 for each of the three growth conditions. It is very difficult to judge the overall impact on the "preferable" ribbon orientations directly from the diffraction patterns, or even somewhat from TC values. The T_{Source} = 400 °C, T_{Sub} = 350 °C device has the highest unfavourable (020) coefficient and lower TC for the favourable (002), (211) and (221) peaks. By calculating the RCT values we can simplify this analysis though. The 400 °C/350 °C device has a lower ΣRCT value of 4.5 compared to the other samples of 5.1 and 5.4. It is notable that the highest ΣRCT (i.e. nanoribbons are more vertical) is attained not by increasing the substrate temperature, but by maintaining it at 350 °C and increasing the source temperature. This implies that higher deposition rate, as achieved by increased source temperature, has more of a controlling factor than substrate temperature.

The seed layer films were then processed into complete devices via addition of P3HT/Au contact grids. The cells performance parameters were measured via JV analysis and shown in Fig. 5. JV and EQE curves for the highest efficiency contacts from each device are given in Fig. 6, with associated peak performance parameters in Table 4. The higher substrate temperature sample at T_{sub} = 390 °C produced significantly poorer performance due to particularly low FF values as can be seen from the shape of the associated JV curve. The highest efficiency recorded was for the higher source temperature with lower substrate temperature (T_{Source} = 440 °C with T_{Sub} = 350 °C) at 4.45 % but this sample showed a much greater degree of variance in device performance. This is likely attributable to the void regions visible in Fig. 3b, meaning a number of shunted regions may be formed which impact performance of certain contacts the lower temperature combination sample (T_{Source} = 400 °C with T_{Sub} = 350 °C) had much more consistent performance and also had a significantly improved V_{oc} at 0.43 V compared to <0.41V for the other samples. The primary improvement for the peak performance device was due to an increased J_{sc} for the T_{Source} = 440 °C with T_{Sub} = 350 °C device. From the EQE, it can be seen that there are losses across all optical spectrum rather than in a particular range, indicating that losses were due to poor optical absorption or interfacial reflection losses.

Comparing device performance to our ΣRCT values we see that the device with the lowest ΣRCT has the highest V_{OC}. High V_{OC} is typically taken as a marker of overall material quality so clearly a poorer ribbon orientation has not overtly impacted performance. It may be that the relative orientations fall within a "tolerable" orientation range which is not sufficiently poor to compromise carrier transport. The improved V_{oc} may instead relate to the significantly larger grain size of for this device. Whilst Sb_2Se_3 is believed to have a degree of grain boundary defect tolerance [22], one will still anticipate a reduction in presence of grain boundaries to be beneficial as observed for other materials such as CdTe [30]. For this device series increasing the grain size appears to have been beneficial for V_{OC}.

There are two takeaways from this initial device series. Firstly, it is possible to get respectable device efficiency, in particular V_{oc}, using a

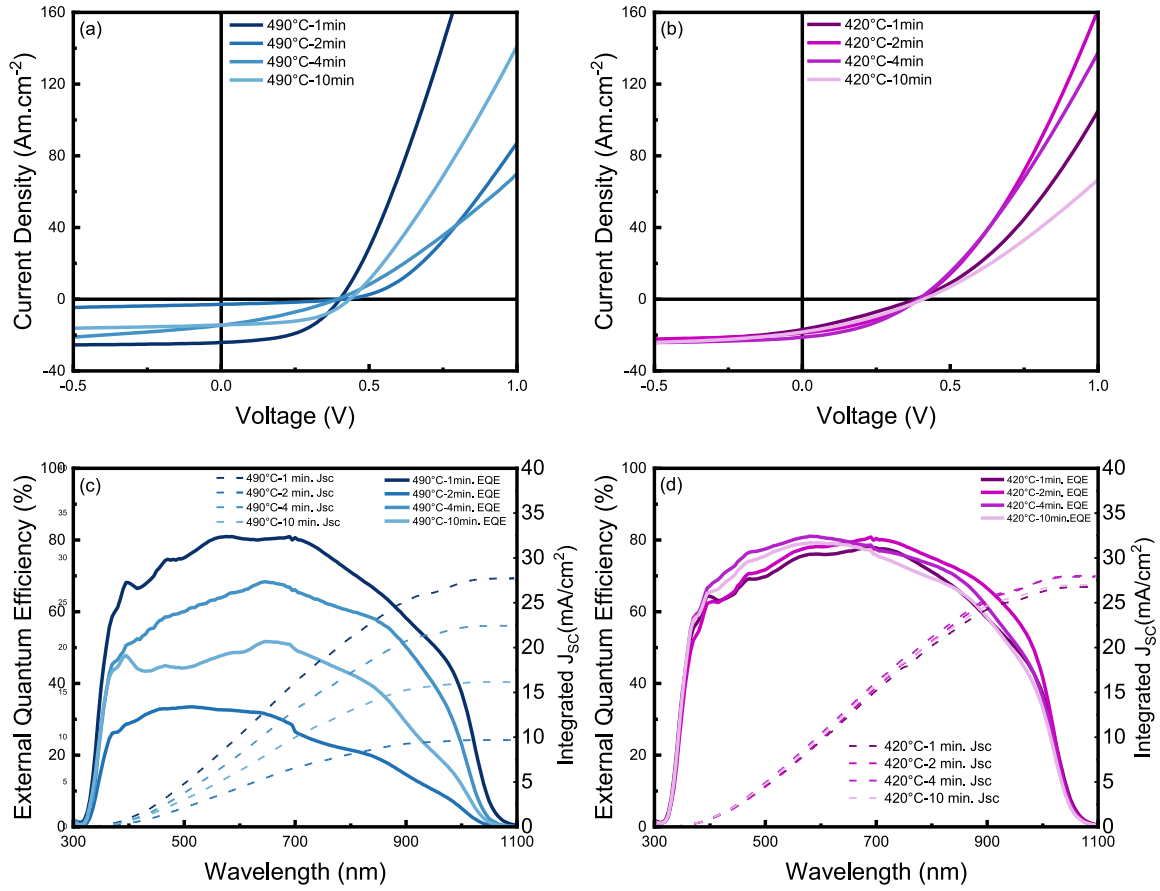

Fig. 10. a), b) JV and c), d) EQE analysis with integrated J_{sc} of highest efficiency contacts from devices with absorber layers deposited for various deposition times and at substrate temperatures of either a),c) 420 °C or b), d) 490 °C.

single lower temperature deposition step, something not possible from a single high temperature deposition step. Secondly, we see a large variance in V_{oc} and no evidence that ribbon orientation is a controlling factor. Instead it appears that overall grain size may be more important.

3.3. Two-step deposition process

The prior sections established that a seed layer was essential for production of good quality films but also that single step seed layer films could produce functional devices. This section seeks to establish the degree of control that the second growth layer step has on ribbon orientation, grain structure and subsequent device performance. Here the seed layer condition was fixed was at $T_{source} = 440$ °C and $T_{substrate} = 350$ °C deposited under vacuum for a duration of 17 min. For the second growth step a fixed source temperature of 530 °C was used with a nitrogen pressure of 10 Torr. A series of devices was then produced with substrate temperatures of either 420 °C and 490 °C each for deposition times of 1, 2, 4 and 10 min. The decision was taken to use comparable deposition times rather than absorber thicknesses due to the unpredictable variation in measured film thickness for different substrate temperatures due to the rough surface of the Sb_2Se_3 films. This is exemplified by the measured absorber thicknesses presented in Table 5 which do not show a linear progression with time one may expect. This may imply that there is a significant amount of recrystallisation and grain growth, or indeed some re-evaporation from the surface, occurring during the early stages of the higher temperature deposition step.

Fig. 7 shows the SEM images of all films produced. The top row of Fig. 7 displays films deposited at the higher substrate temperature of 490 °C. These films show an increase in grain size longer deposition time, but also progressively worse substrate coverage. By decreasing the substrate temperature to 420 °C (bottom row of Fig. 7), we do not observe as pronounced a reordering of the grain structure with increased deposition time with good coverage being maintained. There are also some pyramidal grains visible in both series, but particularly apparent in Fig. 7g, which can be attributed to oxide phases.

Fig. 8 shows the XRD and TC for the sample series. Firstly, it is notable that in all 8 films the XRD result confirms the presence of some Sb_2O_3. This is attributable to the low vacuum conditions of the CSS process and the pyramidal grains observed in the SEM results are confirmed to be an oxide phase via the use of EDS analysis (Fig. S1). Despite the established benefits to contacting of oxygen incorporation at the Sb_2Se_3 back surface [32], large oxide regions are undesirable. However, no correlation between such phases and reduced device performance was observed although their influence warrants further study.

In contrast to prior samples the TC analysis demonstrates a complete absence of unfavourable (020) texture from all films in the series, although the (130) peak remains. Beyond this it is difficult to make a comparison to previous sample series from TC values alone so again RCT analysis provides a simplified comparison. This analysis was conducted for all samples with ΣRCT values summarized in Table 6. Comparing the determined values, we see that the addition of the second growth step has improved the overall film orientation. It is also notable that despite the large change in substrate temperature and deposition time the ΣRCT values remarkably consistent in the 6.1–6.4 range. The overall verticality of ribbon orientation has therefore been improved compared to the single step lower temperature seed deposition, primarily due to the lack of certain (hk0) planes.

Fig. 9 shows the JV parameters of Sb_2Se_3 solar cells fabricated under two different growth temperatures, with highest efficiency contacts parameters summarized in Table 7. There is little change in the peak

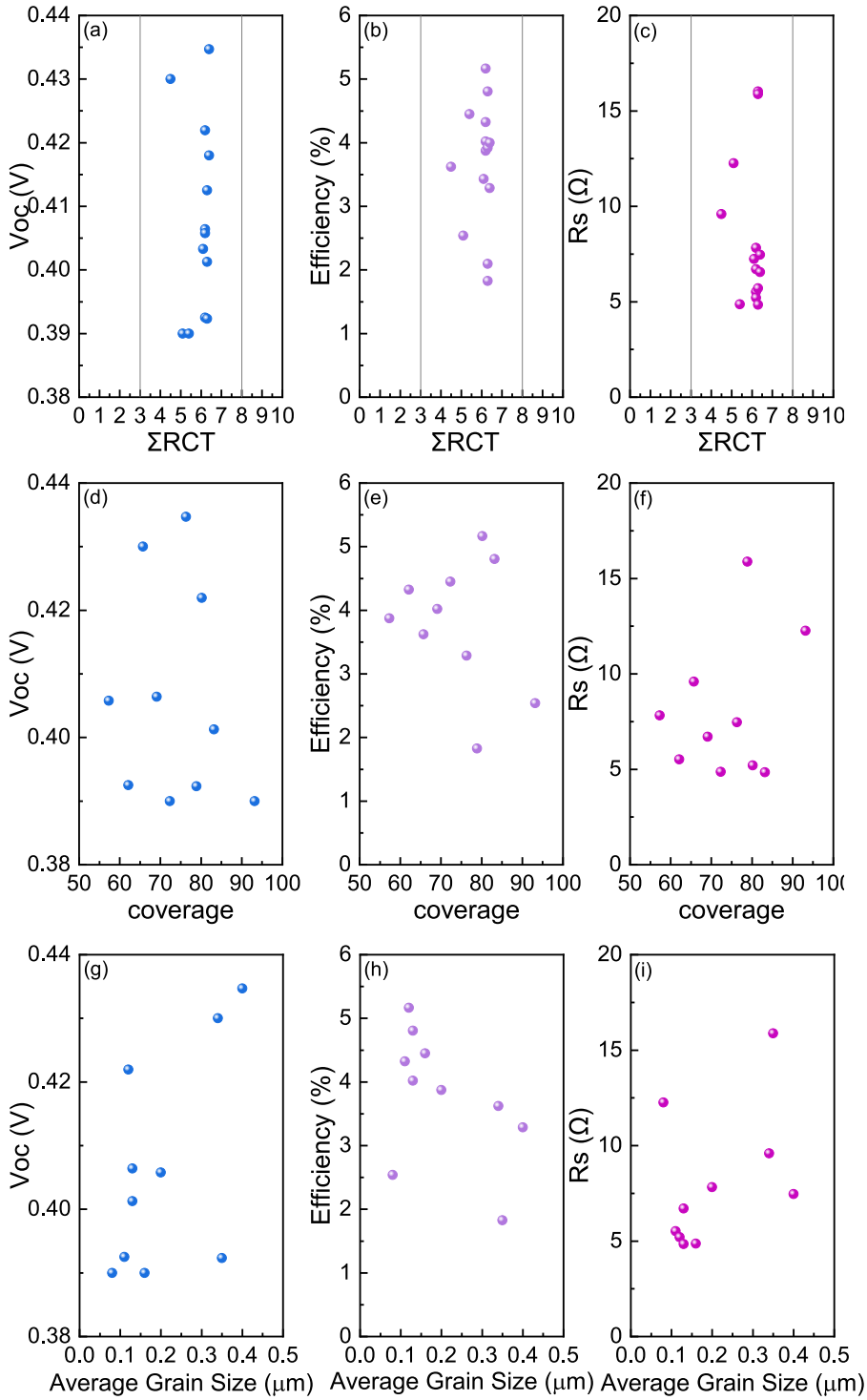

Fig. 11. Comparison of V_{oc} (a,d,h), efficiency (b,e,h) and R_S (c,f,i) versus ΣRCT (top), substrate coverage (middle) and average grain size (bottom) for all films analysed in this study.

performance due to changing the substrate temperature, with the lower substrate temperature performance being marginally higher due to a slight J_{SC} increase. Some variation is seen as a function of deposition time particularly for the 490 °C. Highest efficiency is obtained for a 1 min deposition time before a rapid decrease in performance. This is presumed to be the large amount of grain re-ordering observed and significant shunting due to void regions. Large losses in can be seen via the decrease in EQE and integrated J_{sc} (Fig. 10c) For the 420 °C device performance is more consistent as a function of deposition time, which correlates with less overall change to the grain structure. Both high and low substrate temperature devices do show increased V_{oc} for longer deposition times. Again, there appears to be little obvious relation between device performance and RCT value. Despite showing an improved ΣRCT compared to the seed layer samples, and lack of (002) or (120) texture, we see only a minor increase in efficiency but for the peak performing devices the V_{oc} has decreased from 0.43V to 0.40V. In contrast we see larger grain size devices (Figs. 3c and 7d) seem to have higher V_{oc}.

To better determine any overall relationship between device performance and film structure, the device efficiency, V_{OC} and R_S are plotted against ΣRCT, average grain size and level of substrate coverage for all devices measured in this work is given in Fig. 11. For the ΣRCT analysis (Fig. 11a–c) the findings show that despite the wide range of deposition conditions used throughout this study, the value of the ΣRCT falls within the mid-range of 4.5%–6.4 %. This indicates that irrespective of deposition temperatures chosen, CSS deposition appears to produce films of reasonably "good" ribbon orientation (i.e large vertical component). Whilst the addition of a second deposition step does improve orientation, increasing ΣRCT above 6 and improving efficiency, it is difficult to conclude there is a direct correlation between performance and orientation as has been previously reported [14]. Likewise, the level of surface coverage appears to have no discernible trend on any of the parameters assessed. This is somewhat surprising but we would anticipate this to be a more dominant factor in the absence of the P3HT back contact layer which serves to block pinhole shunting [17]. For the grain size analysis there is some slight indication that smaller grain sizes may be more favourable for high efficiency, with all the highest efficiency devices being of a grain size <0.2 μm. However, given the small number of samples with grain sizes larger than this, it is by no means conclusive. Instead these results suggest that rather than there being a decisive factor controlling efficiency such a ribbon orientation, it is the overall grain structure, including grain size, coverage and orientation, that determines device performance for CSS deposited Sb_2Se_3.

4. Conclusions

We have presented a comprehensive investigation into the influence of one and two stage growth approaches for CSS deposition of Sb_2Se_3. A low temperature "seed" layer was demonstrated to be essential to achieving the required level of substrate coverage to form functional devices. Whilst a seed layer in isolation was shown to be capable of producing devices of >4 % efficiency, addition of a second-high temperature step improved the performance to >5 %. Comparisons were made between device performance, ribbon orientation, substrate coverage and grain size with no single factor found to be dominant. No specific ribbon orientations were found to be necessary to achieve high performance and instead overall grain structure may be a more dominant factor. This study demonstrates that control over grain orientation in Sb_2Se_3 films is complex, and it is extremely difficult to control one variable (i.e. grain orientation) without affecting many other variables incidentally (as shown here for substrate coverage, thickness, grain size, crystallinity etc), which could account for some of the correlations between device performance and grain orientation found in literature. A large amount of focus within the research field has been devoted to control of ribbon orientation but we would suggest any performance changes that are identified must be carefully and thoroughly decoupled from the impact of other variables such as grain microstructure. This work suggests a more concerted effort on overall grain structure control, rather than simply ribbon orientation, would be worth pursuing.

CRediT authorship contribution statement

Daniya A. Sindi: Writing – review & editing, Writing – original draft, Investigation, Formal analysis. **Thomas P. Shalvey:** Formal analysis. **Jonathan D. Major:** Writing – review & editing, Supervision.

Declaration of competing interest

The authors declare that they have no known competing financial interests or personal relationships that could have appeared to influence the work reported in this paper.

Data availability

Data will be made available on request.

Acknowledgements

Funding for the work was provided by the Engineering and Physical Sciences Research Council via Grants EP/W03445X/1. Data supporting the project is available from the University of Liverpool data catalouge under project ID #2594 or from the authors.

Appendix A. Supplementary data

Supplementary data to this article can be found online at https://doi.org/10.1016/j.mssp.2024.108161.

References

[1] K. Zeng, D.-J. Xue, J. Tang, Antimony selenide thin-film solar cells, Semicond. Sci. Technol. 31 (2016) 063001.
[2] C. Zhang, J. Zhong, Tang, J. Cu 2 ZnSn (S, Se) 4 thin film solar cells fabricated with benign solvents, Front. Optoelectron. 8 (2015) 252–268.
[3] S. Giraldo, et al., Progress and perspectives of thin film kesterite photovoltaic technology: a critical review, Adv. Mater. 31 (2019) 1806692, https://doi.org/10.1002/adma.201806692.
[4] B.G. Mendis, et al., Direct observation of Cu, Zn cation disorder in Cu2ZnSnS4solar cell absorber material using aberration corrected scanning transmission electron microscopy, Prog. Photovoltaics Res. Appl. 22 (2014) 24–34, https://doi.org/10.1002/pip.2279.
[5] C. Chen, et al., Characterization of basic physical properties of Sb2Se3 and its relevance for photovoltaics, Front. Optoelectron. 10 (2017) 18–30, https://doi.org/10.1007/s12200-017-0702-z.
[6] A.P. Torane, C.H. Bhosale, Preparation and characterization of electrodeposited Sb2Se3 thin films from non-aqueous media, J. Phys. Chem. Solid. 63 (2002) 1849–1855, https://doi.org/10.1016/S0022-3697(02)00167-1.
[7] T.M. Razykov, et al., Growth and characterization of Sb2Se3 thin films for solar cells, Sol. Energy 173 (2018) 225–228, https://doi.org/10.1016/j.solener.2018.07.082.
[8] Y. Zhou, et al., Solution-processed antimony selenide heterojunction solar cells, Adv. Energy Mater. 4 (2014) 1301846, https://doi.org/10.1002/aenm.201301846.
[9] Y. Zhao, et al., Regulating deposition kinetics via a novel additive-assisted chemical bath deposition technology enables fabrication of 10.57%-efficiency Sb2Se3 solar cells, Energy Environ. Sci. 15 (2022) 5118–5128, https://doi.org/10.1039/D2EE02261C.
[10] X. Wang, Z. Li, S.R. Kavanagh, A.M. Ganose, A. Walsh, Lone pair driven anisotropy in antimony chalcogenide semiconductors, Phys. Chem. Chem. Phys. 24 (2022) 7195–7202, https://doi.org/10.1039/d1cp05373f.
[11] L.J. Phillips, et al., Current enhancement via a TiO2 window layer for CSS Sb2Se3 solar cells: performance limits and high Voc, IEEE J. Photovoltaics 9 (2019) 544–551, https://doi.org/10.1109/JPHOTOV.2018.2885836.
[12] H. Lei, J. Chen, Z. Tan, G. Fang, Review of recent progress in antimony chalcogenide-based solar cells: materials and devices, Sol. RRL 3 (2019) 1900026, https://doi.org/10.1002/solr.201900026.
[13] O.S. Hutter, L.J. Phillips, K. Durose, J.D. Major, 6.6% efficient antimony selenide solar cells using grain structure control and an organic contact layer, Sol. Energy Mater. Sol. Cell. 188 (2018) 177–181, https://doi.org/10.1016/j.solmat.2018.09.004.
[14] Y. Zhou, et al., Thin-film Sb2Se3 photovoltaics with oriented one-dimensional ribbons and benign grain boundaries, Nat. Photonics 9 (2015) 409–415, https://doi.org/10.1038/nphoton.2015.78.
[15] M.D. Coutts, E.R. Levin, Phase transformation of As2Se3 and Sb2Se3 films, J. Appl. Phys. 38 (2004) 4039–4044, https://doi.org/10.1063/1.1709063.
[16] T.D.C. Hobson, K. Durose, Protocols for the Miller indexing of Sb2Se3 and a non-x-ray method of orienting its single crystals, Mater. Sci. Semicond. Process. 127 (2021) 105691, https://doi.org/10.1016/j.mssp.2021.105691.
[17] J.D. Major, et al., P3HT as a pinhole blocking back contact for CdTe thin film solar cells, Sol. Energy Mater. Sol. Cell. 172 (2017) 1–10, https://doi.org/10.1016/j.solmat.2017.07.005.
[18] A. Amin, et al., Enhanced efficiency and stability in Sb2S3 seed layer buffered Sb2Se3 solar cells, Adv. Mater. Interfac. 9 (2022) 2200547, https://doi.org/10.1002/admi.202200547.
[19] A. Amin, et al., Heterostructured CdS buffer layer for Sb2Se3 thin film solar cell, Sol. RRL 7 (2023) 2300417, https://doi.org/10.1002/solr.202300417.
[20] F. Pattini, et al., Role of the substrates in the ribbon orientation of Sb2Se3 films grown by Low-Temperature Pulsed Electron Deposition, Sol. Energy Mater. Sol. Cell. 218 (2020), https://doi.org/10.1016/j.solmat.2020.110724.
[21] N. Spalatu, et al., Screening and optimization of processing temperature for Sb2Se3 thin film growth protocol: interrelation between grain structure, interface intermixing and solar cell performance, Sol. Energy Mater. Sol. Cell. 225 (2021) 111045.

[22] R.E. Williams, et al., Evidence for self-healing benign grain boundaries and a highly defective Sb2Se3–CdS interfacial layer in Sb2Se3 thin-film photovoltaics, ACS Appl. Mater. Interfaces 12 (2020) 21730–21738, https://doi.org/10.1021/acsami.0c03690.
[23] C.H. Don, T.P. Shalvey, J.D. Major, What Can ${\mathrm{Sb}}_{2}{\mathrm{Se}}_{3}$ Solar Cells Learn from $\mathrm{Cd}\mathrm{Te, PRX Energy 2 (2023) 041001, https://doi.org/10.1103/PRXEnergy.2.041001.
[24] W.K. Metzger, et al., Exceeding 20% efficiency with in situ group V doping in polycrystalline CdTe solar cells, Nat. Energy 4 (2019) 837–845, https://doi.org/10.1038/s41560-019-0446-7.
[25] C.H. Don, et al., Multi-phase sputtered TiO2-induced current–voltage distortion in Sb2Se3 solar cells, Adv. Mater. Interfac. 10 (2023) 2300238, https://doi.org/10.1002/admi.202300238.
[26] T.P. Shalvey, H. Bagshaw, J.D. Major, Interrelation of the CdTe grain size, postgrowth processing, and window layer selection on solar cell performance, ACS Appl. Mater. Interfaces 14 (2022) 42188–42207, https://doi.org/10.1021/acsami.2c07609.
[27] G.B.X. Harris, Quantitative measurement of preferred orientation in rolled uranium bars, London, Edinburgh Dublin Phil. Mag. J. Sci. 43 (1952) 113–123, https://doi.org/10.1080/14786440108520972.
[28] P.B. Barna, M. Adamik, Fundamental structure forming phenomena of polycrystalline films and the structure zone models, Thin Solid Films 317 (1998) 27–33, https://doi.org/10.1016/S0040-6090(97)00503-8.
[29] J. Luschitz, et al., CdTe thin film solar cells: interrelation of nucleation, structure, and performance, Thin Solid Films 517 (2009) 2125–2131.
[30] J.D. Major, Y.Y. Proskuryakov, K. Durose, G. Zoppi, I. Forbes, Control of grain size in sublimation-grown CdTe, and the improvement in performance of devices with systematically increased grain size, Sol. Energy Mater. Sol. Cell. 94 (2010) 1107–1112.
[31] R. Kondrotas, J. Zhang, C. Wang, J. Tang, Growth mechanism of Sb2Se3 thin films for photovoltaic application by vapor transport deposition, Sol. Energy Mater. Sol. Cell. 199 (2019) 16–23, https://doi.org/10.1016/j.solmat.2019.04.024.
[32] N. Fleck, et al., How oxygen exposure improves the back contact and performance of antimony selenide solar cells, ACS Appl. Mater. Interfaces 12 (2020) 52595–52602, https://doi.org/10.1021/acsami.0c14256.